CRITICAL CURRENT DENSITIES AND *N*-VALUES OF MgB_2 CONDUCTORS FOR SMES, MRI, AND LOW AC LOSS APPLICATIONS

J. Kwon[1], J. Rochester[1], F. Wan[1,2], M.A. Rindfleisch[3], M.J. Tomsic[3], M.D. Sumption[1], and E.W. Collings[1]
[1]Center for Superconducting and Magnetic Materials, The Ohio State University, Columbus, OH 43210
[2]Now employed at Fermilab, Batavia, IL 60510
[3]Hyper Tech Research, Columbus, OH 43228

***Abstract*—Multifilamentary MgB_2 strands (filament numbers 36 to 114) prepared by the in-situ power-in-tube (PIT) route with carbon doping contents of 0, 2, and 3.2% were wound on barrels for transport J_c and *n*-value measurement at 4.2 K in fields of up to 12 T. The strand and gauge lengths were 1 m and 0.5 m. Heat treatments at 675 °C and 650 °C centered around the melting point of Mg (650 °C) and both utilized the liquid-solid reaction. A pair of strands, with and without 2% C doping exhibited the J_c (B) crossover effect. Studied were the dependencies of J_c on field strength, dopant concentration, and cabling and the dependence of *n*-value on field strength.**

***Index Terms*—Cabling, Carbon Doping, MgB_2,**

I. INTRODUCTION

MAGNESIUM DIBORIDE, with a T_c of about 39 K can be classified as a medium temperature superconductor [1]. As such it can be cooled by a cryocooler which eliminates the need for liquid helium. Commercial applications of MgB_2 include cables for superconducting magnetic energy storage (SMES), magnetic resonance imaging (MRI), and low AC loss cables for motors and generators [2-5].

Since its discovery of MgB_2 in 2001, numerous studies have resulted in improvements to the overall performances of superconducting strands and cables. Basic wire fabrication techniques investigated were in-situ powder-in-tube (PIT) [6,7], ex-situ PIT [8,9] and advanced internal magnesium infiltration, known as AIMI [10-14]. Under AIMI an axially positioned Mg rod melts, diffuses into, and reacts with a surrounding B layer. Under in-situ PIT, the technique used here, the starting tube is filled with a suitable ratio of Mg, B, and dopant powders in preparation for wire drawing and heat treatment [15].

Numerous small percentages of dopant have been mixed with the starting Mg+B powders in attempts to improve the performance of MgB_2 strands. A very successful dopant is C which as shown here and elsewhere [16-18] increases the high field J_c. The performance of MgB_2 also depends on the structure of the strand: (i) Pure Cu with its high electrical conductivity at low temperatures helps to stabilize the conductor. (ii) Intrafilamentary CuNi with its high electrical resistivity contributes to lowering the AC loss. (iii) Wire drawing to fine multifilament diameters lowers hysteretic loss but permits an applied AC field to generate eddy currents. (iv) This problem can be diminished by twisting the strand but this often leads to low *n*-values, giving an undesirable normal component to the superconductor as J approaches J_c [19]. (v) The smaller wire diameter lowers the strand's transport current which can be restored by cabling together a bundle of strands. (vi) The electrical contacts between the strands of the cable permit the generation of coupling currents.

II. EXPERIMENTAL

A. Sample Preparation

Multifilamentary MgB_2 strands with carbon doping contents of 0 at%, 2 at%, and 3.2 at% and filament numbers of 36 to 114 were manufactured by HyperTech Research (HTR) by the in-situ power-in-tube (PIT) route. The B powder sources were PVZ (Pavezyum Chemical Company) and SMI (Specialty Metals Inc). Various samples were reaction-heat-treated at the optimum heat-treatment for PIT strands for 1h at 650 °C and 1h at 675 °C. The same heat-treatment is applied to all the strands despite the differences in filament sizes and matrix materials. Conductor types suitable for SMES, MRI, and AC applications in the form of individual strands, 3-strand cables (SMES), and 7-strand cables (AC), respectively were prepared for measurement. The 3-strand and the 7-strand cables are constructed as a triplet and a 6 around 1 respectively. Additional construction parameters are shown in Figure 1.

B. Measurement Procedure

Strand and cable samples for transport J_c (B) measurement were wrapped helically around a modified ITER barrel made of Ti-6-4 and soldered onto Cu end rings for current transfer to the probe. The conductor and gauge lengths were 1 m and 0.5 m. Measurements of J_c and *n*-value took place in fields of up to 12 T at 4.2 K in pool-boiling liquid helium using electric field criteria of 1.0 μV/cm and 0.1 μV/cm.

TABLE I: STRAND SPECIFICATIONS

Strand	Internal #	# Strands	# Fil-ament	Mono and Central Sheath	Multi Sheath	Dopants	B type	% MgB_2	HT °C/hr	OD (mm)	Twist Pitch Strand/Cable (mm)
SMES1	E4013	1	54	Cu10Ni	Cu30Ni	3.2 at% C	PVZ	11	675/1	1.01	100
SMES2	E4137	3	54	Cu10Ni	Cu30Ni	3.2 at% C	PVZ	11	650/1	0.52	10/25
MRI1	E3929	1	36	Cu	Monel	N/A	PVZ	10	675/1	0.84	N/A
MRI2	E3476	1	54	Cu	Monel	2 at% C	SMI	10	650/1	0.84	100
LL1	E4067	1	54	Cu30Ni	Cu30Ni	N/A	SMI	10	650/1	0.85	10
LL2	E3930	1	114	Cu30Ni	Cu30Ni	N/A	SMI	9	650/1	0.85	10
LL3	E4116	7	54	Cu30Ni	Cu30Ni	N/A	SMI	8	650/1	0.29	10/10

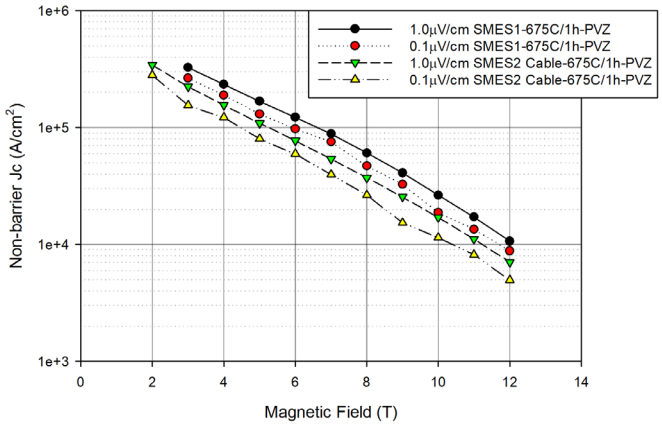

Figure 1: J_c versus B for SMES1 and SMES2 measured at 1 μV/cm and 0.1 μV/cm

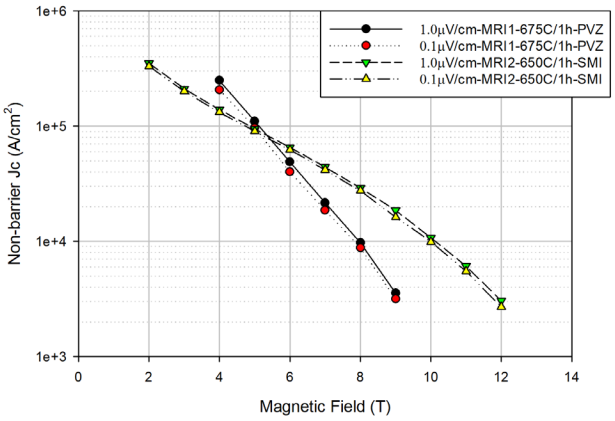

Figure 2: J_c versus B for MRI1 and MRI2 measured at 1 μV/cm and 0.1 μV/cm

The instrumentation includes Oxford Instruments 12T magnet with Hewlett Packard multimeter for data acquisition. Quench detection system is managed by a Keithley Sensitive Digital Voltmeter to detect a quench and send a direct emergency stop to the power supply to prevent damage to the wires.

III. RESULTS

A. The SMES Conductors SMES1 and SMES2

Figure 1 displays $J_c(B)$ for SMES1 and SMES2 at electric fields of 1.0 μV/cm and 0.1 μV/cm. Both strands have 54 filaments in a Cu10Ni matrix. The Mg to PVZ B ratio was 1.15:2 and the B powders were pre-doped with 3.2 % C by the manufacturer. The heat treatments were 675 °C/1 h (SMES1) and 650 °C/1 h (SMES2). Notable is a uniform decrease in $J_c(B)$ over the whole field range. In particular at 5 T J_c (1.0 μV/cm) decreased from 1.8×10^5 A/cm^2 (SMES1, single strand) to 1.0×10^5 A/cm^2 (SMES2, 3-strand cable). This reduction may stem from several factors including smaller filament sizes and/or cabling degradation. We note that similar strands have shown undiminished performance with filaments counts up to 114 at strand diameters down to 0.6 mm OD [3]. Further clarification is needed here.

B. The MRI Conductors MRI1 and MRI2

Figure 2 displays J_c(B) for single strand samples MRI1 and MRI2 at electric fields of 1.0μV/cm and 0.1μV/cm. To aid stability in MRI applications pure Cu is used for the sheath materials.

In actual practice Cu/SC ratio of up to 20:1 is used – much larger than in the present strands. MRI1 has 36 filaments and MRI2 has 54. They were formed with PVZ B and 2 % C-doped SMI B respectively. MRI1 was designed with no C doping and no twist pitch to test the upper-end performance for PVZ, while MRI2 adapts common fabrication methods for MRI application.

Figure 2 shows MRI1 intersecting MRI2 at 5 T and indicates that of the two strands the undoped MRI1 would be preferable for applications below 5 T and the 2 % C-doped MRI2 for applications above that field. The results also indicate that 3.2 % C-doped SMES1 and SMES2 would also be suitable for high field applications. We note that the slopes of the doped and undoped $J_c(B)$ curves exhibit what is known as the "$J_c(B)$ crossover effect" [20]. In grain-boundary-pinned superconductors dopant additions such as C raise the high field J_c, but at fields small compared to the upper critical field, B_{c2}, $J_c(B)$ decreases as B_{c2} increases. In general, this leads to a convergence, or intersection, of a group of variously doped MgB_2 strands.

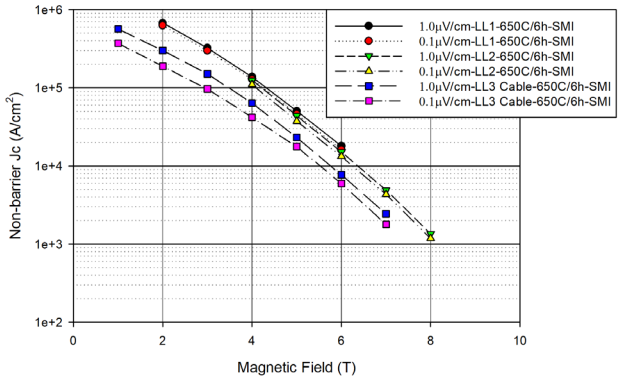

Figure 3: J_c versus B for LL1, LL2, and LL3 measured at 1 μV/cm and 0.1 μV/cm

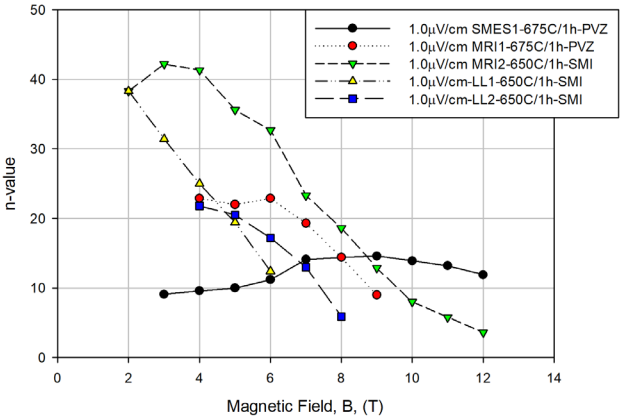

Figure 4: *n*-value versus B for the SMES, MRI, and LL series conductors

C. Low AC Loss Conductors

HTR has been developing low loss conductors for several years paying particular attention to: (i) reducing the filament size (reducing hysteretic loss), (ii) reducing the twist pitch, (iii) increasing the matrix resistivity (to reduce both coupling currents and eddy currents).

In strands LL1, 2, and 3 matrix resistivity was increased by the use of Cu30Ni. In strands LL1 and LL2 reductions in filament diameter, *d*, were achieved by including 54 and 114 filaments in 0.85 mm OD strands. Then since hysteretic loss, Q_h, is proportional to $J_c d$, the selection of J_c for a particular application should be carefully made. For low field applications (e.g., AC machines), doping or non-doping would provide "low" or "high" J_c, respectively. The low low-field J_c (doping) would suppress Q_h at the cost of lower current margin; conversely for high low-field J_c (non-doping), see Figure 2 for clarification. Figure 3 displays $J_c(B)$ for LL1, LL2, and LL3. The curves for the monocores LL1 and LL2 are clustered together while that for the 7-strand cable is significantly lower, possibly as a result of cabling induced degradation. The strands LL1 and LL2, with 54 and 114 filaments exhibit the highest 2 T J_c. But LL3, a cable wound from 7 strands of LL1 has the lowest performance. The reasoning for reduction in LL3 cable is similar to the reduction seen for SMES2. Smaller filament sizes and/or cabling degradation are possible culprits for lowered J_c performance.

TABLE II: J_c (10^5 A/CM^2) VS FIELD (B) AT 4.2 K AT 1 MICROVOLT/CM

Conductor	% C in MgB_2	2T	5T	10T
SMES1	3.2 at%	4.8	1.68	0.26
SMES2	3.2 at%	3.42	1.09	0.17
MRI-1	0	11.0	1.10	0.02
MRI-2	2 at%	3.51	0.95	0.11
LL-1	0	6.75	0.50	0.002
LL-2	0	6.0	0.44	0.002
LL-3	0	3.01	0.23	0.001

D. Critical Current Density and n-Value

Figure 4 displays *n*-value vs *B* for strands SMES-1,2, MRI-1,2, and LL-1,2,3. The majority of *n*-values presented follows a well-studied relationship between J_c and *n*-value [21] that:

$$n = J_c^{\,m} \qquad (1)$$

For *n*-values at mid to high fields, the inverse relationship between *n*-value and B, thus J_c, can be visualized by most of the wires presented despite the different matrix materials and different doping concentrations intended for various applications. The use of PVZ powders does not seem to impact the high field *n*-value. The *n*-value at this range is dependent on the intrinsic effects of increasing flux-pinning forces [22] and all the wires follow the expected inverse relationship with increasing field.

However, at low fields, extrinsic effects [22], including such items as the uniformity of the superconducting cross-sectional area along the length of the wire, control the behavior of the *n*-value. For SMES1, this effect dominates the lower field range and it exhibits a *n*-value only in the 10's throughout the full magnetic field range tested. To reduce AC losses in MgB_2, it required to have a high number of filaments, twisting, and small diameter [23]. Despite the added fabrication demands, SMES1 maintains competitive J_c relative to other set of wires presented.

IV. CONCLUDING SUMMARY

A. Dependence of J_c on Field Strength

For all conductors Table II displays the fall of J_c with increasing applied fields from 2 T to 10 T. It can be seen that C-doping reduces the field dependencies of the J_cs. Those of the undoped PIT strands decrease by roughly ×1000 over this range while those of the C-doped strands drop by only ×35 (2% C) and ×17 (3.2 % C). While doping increases the high field J_c e.g., by 10 it decreases the low field J_c e.g., by 1/20. The difference in slopes of the undoped and doped $J_c(B)$ curves leads to their convergence, or intersection. For example, Figure 2 shows undoped MRI1 intersecting MRI-2 at 5 T and indicates that undoped MRI1 would be preferable for applications below 5 T and the 2% C-doped MRI2 for applications above that field.

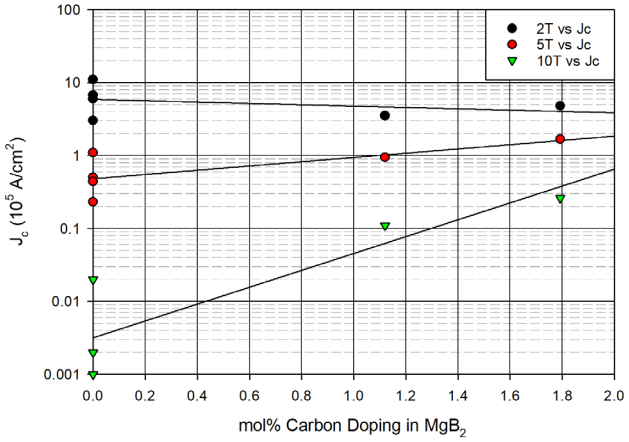

Figure 5: J_c versus C-doping concentration in applied fields of 2 T, 5 T, and 10 T

Figure 5 displays how J_c responds to applied field strength and C-doping concentration. The C-doping contribution was normalized to % C-doping in MgB_2 to avoid any mix-up between wt% and at% for PVZ and SMI classification. While cable construction varied with varying B sources, a general trend can be observed. At low fields J_c responds only weakly to C concentration but at 10 T, J_c benefits strongly from additions of C.

To achieve high current carrying capacity, the combining of individual conductors into a cable is necessary. The advantages and disadvantages of cabling are exemplified by 3-strand SMES2 and 7-strand LL3. Table II shows that cabling SMES1 reduces J_c (5 T and 10 T) by 65% and cabling LL1 reduces J_c (5 T and 10 T) on average by 48%. But in spite of this observed cabling-induced degradation of J_c, the actual transport I_cs were increased by ×2 and ×3.4 respectively. While decreasing wire diameter for cabling has its drawbacks on J_c, it has a reciprocal benefit in decreasing AC losses.

Wires designed for SMES low AC loss demonstrated that different wire matrix material for various AC applications was able to keep up with high performance MRI wires in J_c measurements despite higher resistivity matrix of both Cu10Ni and Cu30Ni.

B. Dependence of n-Value on Field Strength

The *n*-value shows the quality factor of the wire for both intrinsic and extrinsic effects. While many followed the general form of decreasing with *B*, SMES displayed lower than average *n*-values. This is due to its extrinsic effect in the low to mid field range. Its low n-value is not determined by the new B source, PVZ, but contribution from both decreased filament size and cabling degradation from preheat-treatment torsion strain creates nonuniform cross-sectional areas of MgB_2 thus impacting the uniformity of the wires.

C. Acknowledgements

This work is supported by the NIH, National Institute of Biomedical Imaging and Bioengineering, under grant R01EB018363, and NASA, SBIR, under grant 20-2-A1.04-6812 GRC.

REFERENCES

[1] J. Nagamatsu, N. Nakagawa, T. Muranaka Y. Zenitani, and J. Akimitsu, "Superconductivity at 39 K in magnesium diboride", Nature, 410 63–64, 2001.

[2] K. Vinod, R. G. A. Kumar, and U. Syamaprasad, "Prospects for MgB_2 superconductors for magnet application," Supercond. Sci. Technol., vol. 20, no. 1, pp. R1–R13, Jan. 2007, doi: 10.1088/0953-2048/20/1/R01.

[3] F. Wan, M.D. Sumption, M.A. Rindfleisch, M.J. Tomsic, and E.W. Collings, "Architecture and Transport Properties of Multifilamentary MgB_2 Strands for MRI and Low AC Loss Applications" IEEE Trans. Applied Supercond. 27 6200105 (5pp) (2016)

[4] J. H. Choi, D. G. Lee, J. H. Jeon, E. J. Lee, M. Maeda, and S. Choi, "Customized MgB2 Superconducting Wire Toward Practical Applications at Sam Dong in Korea," J. Supercond. Nov. Magn., vol. 32, no. 5, pp. 1219–1223, May 2019, doi: 10.1007/s10948-018-4814-5.

[5] H. Tanaka et al., "Conduction Cooled MgB2 Coil in Maximum Self Magnetic Flux Density 2.3 Tesla Made with 300-Meter-long Multifilamentary MgB2 Wire," IEEE Trans. Appl. Supercond., pp. 1–1, 2016, doi: 10.1109/TASC.2016.2643443.

[6] W. Goldacker, S.I. Schlachter, B. Obst, and M. Eisterer, "In situ MgB_2 round wires with improved properties", Supercond. Sci. Technol. 17 S490 (2004)

[7] B. A. Glowacki, M. Majoros, M. Vickers, J. E. Evetts, Y. Shi, and I. McDougall, "Superconductivity of powder-in-tube MgB_2 wires," *Supercond. Sci. Technol.*, vol. 14, no. 4, pp. 193–199, Apr. 2001, doi: 10.1088/0953-2048/14/4/304.

[8] V. Braccini, D. Nardelli, R. Penco, and G. Grasso, "Development of ex situ processed MgB_2 wires and their applications to magnets", Physica C: Superconductivity 456, 209-217 (2007)

[9] A. V. Pan, S. Zhou, H. Liu, and S. Dou, "Properties of superconducting MgB_2 wires: in situ versus ex situ reaction technique," Supercond. Sci. Technol., vol. 16, no. 5, pp. 639–644, May 2003, doi: 10.1088/0953-2048/16/5/317.

[10] F. Wan, M.D. Sumption, M.A. Rindfleisch, C.J. Thong, M. Tomsic, and E.W. Collings," High performance, advanced-internal-magnesium-infiltration (AIMI) MgB_2 wires processed using a vapor-solid reaction route" Supercond. Sci. Technol. 33, 0994004 (15pp) (2020)

[11] G. Giunchi, "THE REACTIVE Mg-LIQUID INFILTRATION TO OBTAIN LONG SUPERCONDUCTING MgB2 CABLES," *Cryogenics*, vol. 46, no. 2–3, pp. 237–242, 2006.

[12] J. M. Hur, K. Togano, A. Matsumoto, H. Kumakura, H. Wada, and K. Kimura, "Fabrication of high-performance MgB_2 wires by an internal Mg diffusion process," Supercond. Sci. Technol., vol. 21, no. 3, p. 032001, Mar. 2008, doi: 10.1088/0953-2048/21/3/032001.

[13] Y. Liu, F. Cheng, W. Qiu, Z. Ma, M. S. Al Hossain, and S. X. Dou, "High performance MgB_2 superconducting wires fabricated by improved internal Mg diffusion process at a low temperature," J. Mater. Chem. C, vol. 4, no. 40, pp. 9469–9475, 2016, doi: 10.1039/C6TC03288E.

[14] Y. Liu, F. Cheng, Q. Cai, W. Qiu, Y. Lu, and Z. Ma, "The kinetics mechanism of MgB2 layer formation within MgB2 superconducting wire fabricated using improved internal Mg diffusion process," J. Alloys Compd., vol. 697, pp. 37–42, Mar. 2017, doi: 10.1016/j.jallcom.2016.12.133.

[15] G.Z. Li, M.D. Sumption, M.A. Susner, Y. Yang, K.M. Reddy, M.A. Rindfleisch, M.J. Tomsic, C.J. Thong, and E.W. Collings, "The critical current density of advanced internal-Mg-diffusion-processed MgB_2 wires" Supercond. Sci. Technol., 25 115023 (27pp) (2012)

[16] R.H.T. Wilke, S.L. Bud'ko, P.C. Canfield, D.K. Finnemore, R.J. Suplinskas, and S.T. Hannahs, "Systematic effects of carbon doping on the superconducting properties of Mg(B1-xCx)2", Phys. Rev. Lett. 92 217003 (4pp) (2004)

[17] S. Soltanian, J. Horvat, X. L. Wang, P. Munroe, and S. X. Dou, "Effect of nano-carbon particle doping on the flux pinning properties of MgB2 superconductor," Phys. C Supercond., vol. 390, no. 3, pp. 185–190, Jul. 2003, doi: 10.1016/S0921-4534(03)00960-2.

[18] M. Paranthaman, J. R. Thompson, and D. K. Christen, “Effect of carbon-doping in bulk superconducting MgB2 samples,” Phys. C, 2001.
[19] Y. Yang, M.A. Susner, M.D. Sumption, M. A. Rindfleisch, M.J. Tomsic, and E.W. Collings, “Influence of strand design, boron type, and carbon doping method on the transport properties of powder-in-tube MgB_2–xCx strands”, IEEE Trans. Appl. Supercond. 22 6200110 (2012)
[20] M.A. Susner, M.D. Sumption, M.A. Rindfleisch, and E.W. Collings, “Critical current densities of doped MgB_2 strands in low and high applied field ranges: The Jc(B) crossover effect” Physica C: Superconductivity 490 20-25 (2013)
[21] J.H. Kim, S.X. Dou, A. Matsumoto, S. Choi, T. Klyoshi, and H. Kumakura, “Correlation between critical current density and n-value in MgB_2/Nb/Monel superconductor wires”, Physica C: Superconductivity 470 1207-1210 (2010)
[22] D. M. J. Taylor and D. P. Hampshire, “Relationship between the n -value and critical current in Nb_3Sn superconducting wires exhibiting intrinsic and extrinsic behaviour,” Supercond. Sci. Technol., vol. 18, no. 12, pp. S297–S302, Dec. 2005
[23] M.D. Sumption, F. Wan, M. Rindfleisch, and M. Tomsic “AC Loss of Superconducting Materials- Refined Loss Estimates of MgB_2 Wires for Superconducting Motors and Generators”, AIAA/IEEE Electric Aircraft Technologies Symposium doi: 10.2514/6.2018-5001 (2018)